Determining Index Data from Refracted/Diffracted Rays

A report form the 1995 Mathematical Problems in Industry Workshop

Report prepared by:
Jay Bourland
Mathematics Department
Colorado State University
Fort Collins, CO, USA

November 7, 1995

1   Introduction

An optical fiber is a cylindrical waveguide of visible (or near visible) light composed of silica doped with germanium oxide (GeO_2). The guiding is accomplished by varying the level of GeO_2 in the fiber to create an index of refraction in the fiber that varies with the radius of the fiber. The fiber is manufactured by creating a large cane with a radius on the order of centimeters that goes through a sequence of heatings and extrusions until it reaches the finished size, which has a radius on the order of microns.

To assess the quality of optical fibers during their manufacture, it is common to measure the index of refraction of a cane during an intermediate step of the process. The index of refraction varies with the radius of the cane, and is written $n(r)$. The desired profile varies depending on the future use of the optical fiber, but a standard profile is a simple parabola

$$n(r) = n_2 + (n_1 - n_2)\left[1 - \left(\frac{r}{a}\right)^2\right],$$

where a is the radius of the cane. Typical values for n_1 and n_2 are 1.47 and 1.45 respectively. Such a profile is shown in Figure 1. The actual profile in an optical fiber does not match the desired profile due to the way in which optical fibers are manufactured. A glass blank is spun on a lathe while a flame that is fed an appropriate level of silica and GeO_2 moves rapidly back
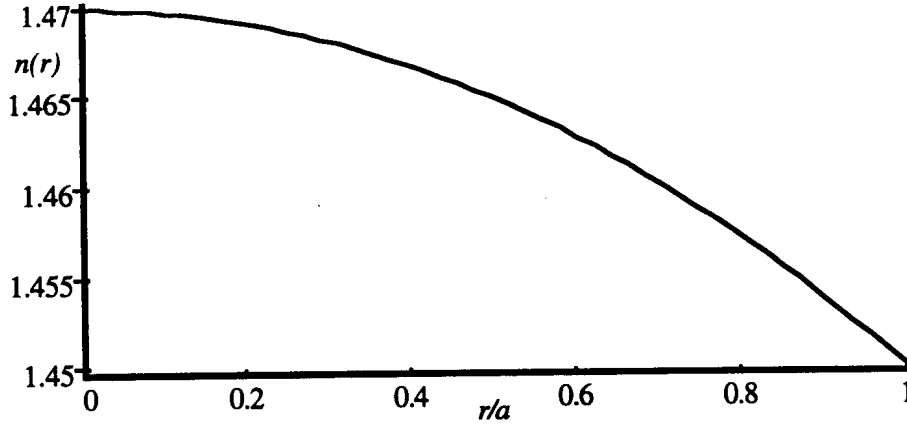
1

Figure 1: A desired parabolic profile for the finished fiber.

and forth along the cane. Soot from the flame is deposited on the spinning blank. Naturally the deposition will create spiral patterns of doping on the cane. This creates oscillations in the level of GeO_2, and therefore in the desired refractive index. Because soot is being deposited at a constant volumetric rate, the wavelength of the oscillation decreases as the radius of the cane increases. The flame travels up and back along the cane in each layer, so the layer structure has two local maxima in each full oscillation. A typical layer structure at three different radial locations inside the cane is shown in Figure 2.

This oscillatory structure inside the fiber is unimportant to the behavior of the fiber, because the wavelength of the oscillation in a fiber of finished size is much smaller than the wavelength of light used in the fiber. However, the oscillations do cause problems when measuring the base index of refraction. The index profile in a cane is typically measured by probing it with a laser [1]. The entering light ray is refracted by the cane and exits with a deflection angle ϕ that varies with the offset of the beam from the centerline of the cane. In a cane without oscillatory layers, all changes in the index of refraction are gradual, and geometrical optics can be used to predict the deflection angle ϕ. The deflection angle of a real fiber with the oscillatory structure described above has a much more complex behavior than the idealized case because the structure within the layers can cause visible effects on the input beam. The deflection within a single input beam will produce an exit beam with a broad structure that makes it difficult to determine the underlying profile.
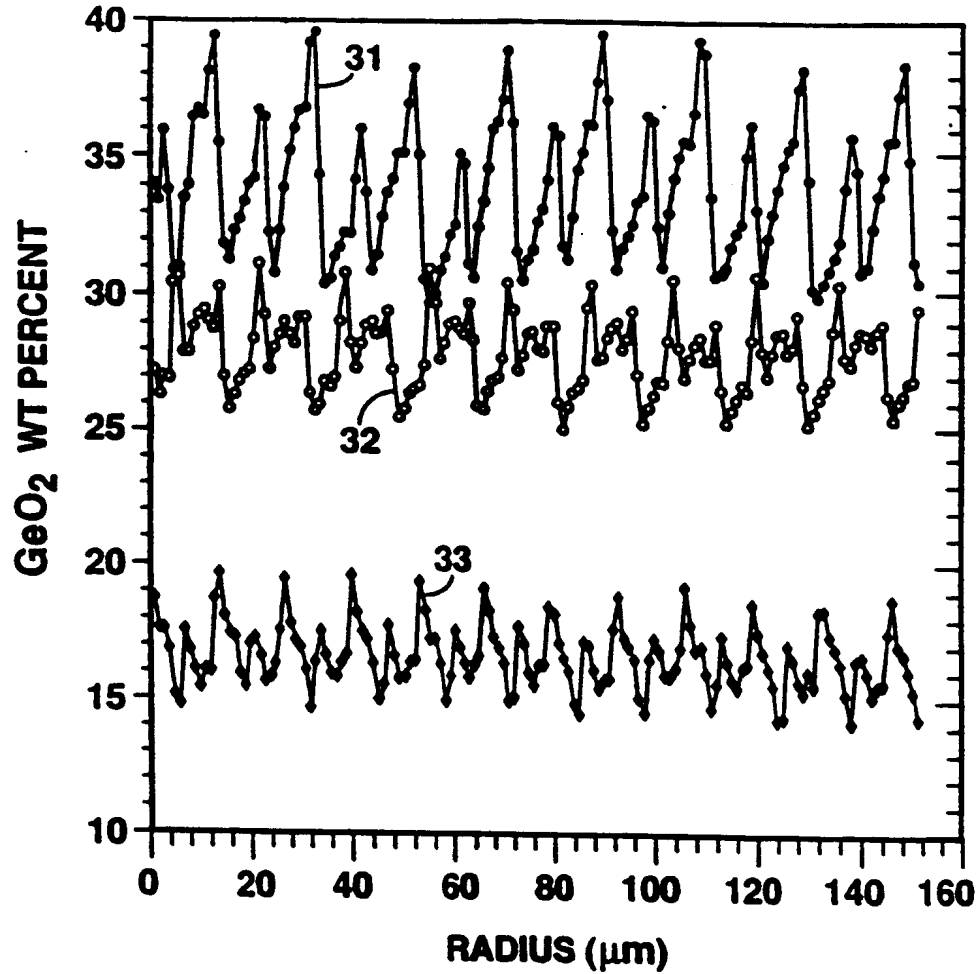
2

Figure 2: The layer structure in a fiber. This figure shows the oscillatory behavior in the doping (and therefore the index of refraction) at three different radii in a fiber. Plot 31 is near the center of the fiber, and 32 and 33 are progressively further out towards the edge. Notice that both the amplitude and wavelength of the fiber decrease as the radius increases.

Because the oscillatory behavior of $n(r)$ is unimportant in the final product, Corning asked MPI '95 to determine a way to remove the noise in the measurements of $n(r)$ caused by the oscillations, and determine the background profile, $n_p(r)$.

2 Improvements to the Model Equations

It was suggested that a simple model for the perturbed index of refraction could be given by the equation:

$$n(r) = n_2 + (n_1 - n_2) \left[1 - \left(\frac{r}{a}\right)^2\right] \left[1 + \epsilon \sin\left(2\pi N \frac{r}{a}\right)\right] . \tag{1}$$

Two improvements were suggested for this model. (1) Since the each layer has two local maxima, the frequency of the perturbation should be doubled (or the first two terms of a representative Fourier series should be used). (2) The deposition of a layer occurs with respect to a constant *volume*, thus a more appropriate variable for the variation is $(r/a)^2$. Then our model would be given by:

$$n(r) = n_2 + (n_1 - n_2) \left[1 - \left(\frac{r}{a}\right)^2\right] \left[1 + \epsilon \sin\left(2\pi N \left(\frac{r}{a}\right)^2\right)\right] . \tag{2}$$

This model gives reasonable agreement with the basic features shown in Figure 2.

3 Geometrical Optics

3.1 Basic Theory

When the variation of the index of refraction is small compared to the wavelength of light, geometrical optics is a well-known technique that may be used to find the path traced by an incoming beam [2]. The basic equation for the ray is given by the Eikonal equation

$$\nabla u \cdot \nabla u = n^2(\mathbf{r}) \,, \tag{3}$$

where $u(\mathbf{r})$ is a function whose contours represent the wave fronts, and $\mathbf{r}$ is the usual position vector. The light rays will follow paths orthogonal to the wavefronts (characteristic paths). The paths are given by

$$\frac{d}{ds}\left(n(\mathbf{r})\frac{d\mathbf{r}}{ds}\right) = \nabla n \,, \tag{4}$$

where s is the arclength along the path. An equivalent form of the ray equation may be derived using calculus of variations and the least-time principle for the ray path. The ray equation (4) is the Euler-Lagrange form of the least-time path.

The ray equation (4) is a system of second-order equations for the coordinates of the ray path. It must also be coupled with the algebraic equation

$$\left|\frac{d\mathbf{r}}{ds}\right| = 1 \tag{5}$$

to determine the ray path.

We make the assumption that the index of refraction depends only on the radial coordinate, $n = n(r)$ so that (4) becomes

$$\left(\frac{dr}{ds}\right)^2 = 1 - \frac{c^2}{r^2 n^2(r)} \tag{6}$$

$$\frac{d\theta}{ds} = \frac{c}{r^2 n(r)} \tag{7}$$

after an integration and an application of (5). The constant c is determined by the initial slope of the ray path. For a horizontal ray entering the cylinder at $r = a$ a at a distance t from the $theta = \pi$ axis, then $c = -t * n(a)$. The problem of interest is to determine the index of refraction from experimental data about the ray paths. Typical data is the deflection of a horizontal beam by the fiber as a function of the offset y_{obs} (see Figure 3). A common method
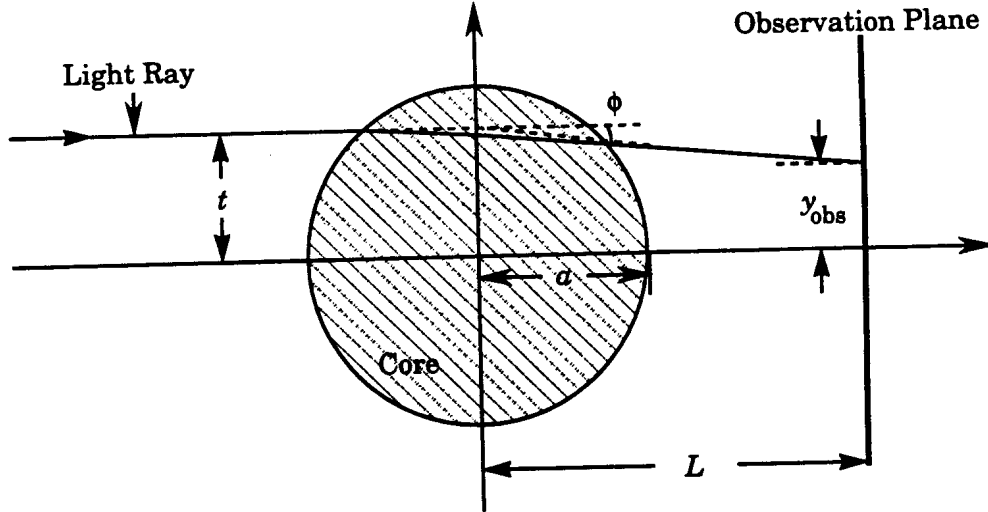
5

Figure 3: The basic setup for the refraction angle method.

based on the ray paths is called the *refraction angle method* as described in [1]. It is based on the fact that deflections of the ray are small for weak refractive-index gradients and short path lengths. When the slope of the ray paths is not large, $y'(x) \ll 1$ where $y(x)$ is the ray path, then $s \approx x$ and $n(r) \approx n_2$. Under these assumptions, the ray equations (6) and (7) reduce to

$$\frac{d^2 y}{dx^2} = \frac{n'(r)y}{n_2 r} \ .$$ (8)

This approximation is usually referred to as the *paraxial* approximation. We consider horizontal rays that enter the fiber at an offset t from the centerline of the fiber, so we may integrate (8) over the fiber to obtain

$$\tan \phi = \frac{1}{n_2} \int_{x_1}^{x_2} \frac{n'(r)y}{r} \, dx \ .$$ (9)

In (9) x_1 and x_2 are the x-coordinates of the points where the ray enters and exits the fiber and the deflection angle ϕ is the ray angle at the exit point. Now the integral is transformed to an integral over r

$$\tan \phi = \frac{1}{n_2} \left(- \int_a^t \frac{n'(r)y}{r} \frac{dx}{dr} \, dr + \int_t^r \frac{n'(r)y}{r} \frac{dx}{dr} \, dr \right) \ .$$ (10)

A second approximation must be made to get (10) into a tractable form. We note that y is approximately constant during its transit of the fiber, so

6

we may use $y = t$ and $x = \sqrt{r^2 - t^2}$ and get

$$\tan \phi = \frac{2t}{n_2} \int_t^a \frac{dn}{dr} \frac{dr}{(r^2 - t^2)^{1/2}} \cdot \tag{11}$$

Note that the two integrals in (10) become equal under this second assumption to produce the factor of 2 in (11). If an observation screen is placed a distance L from the centerline of the fiber and $y(L) = y_{\text{obs}}(t)$ is the measured deflection of the the ray at the observation screen as a function of the input displacement, then

$$\tan \phi = \frac{y_{\text{obs}}(t) - t}{L} + \mathcal{O}(\phi) \tag{12}$$

where $\mathcal{O}(\phi)$ has the usual meaning that the omitted terms are no larger than ϕ. Under the paraxial assumptions used above, ϕ is small so we can use (12) and rewrite (11) as an Abel integral equation

$$\int_t^\infty \frac{d}{dr} [n(r) - n_2] \frac{dr}{(r^2 - t^2)^{1/2}} = \frac{n_2}{2Lt} [y_{\text{obs}}(t) - t] . \tag{13}$$

The extension of the integral in (11) to $[t, \infty)$ is possible since $n(r) = n_2$ for $r \geq a$. Abel integral equations such as (13) have a well-known inversion and we may solve (13) for $n(r) - n_2$ in terms of the data $y_{\text{obs}}(t)$

$$n(r) - n_2 = -\frac{n_2}{\pi L} \int_r^\infty \frac{y_{\text{obs}}(t) - t}{(t^2 - r^2)^{1/2}} \, dt . \tag{14}$$

3.2 Numerical Experiments

To better understand the problems associated with the inversion of the deflection data, several numerical experiments were performed. The first set of experiments focussed on the primary system of equations from geometrical optics, (6) and (7). These equations were integrated numerically using a simple Runge-Kutta integration scheme to find the paths of the rays. The integration is straightforward, except that care must be exercised with regard to the square root that occurs in (6). Each time the right-hand-side of (6) goes through zero, the sign of the square root is reversed. This change results when a ray stops entering the fiber, $dr/ds < 0$, and begins to exit the fiber, $dr/ds > 0$. Several runs were conducted with different oscillation profiles and at different offsets of the input beam. An input beam of light was approximated with a number of rays spread over the approximate
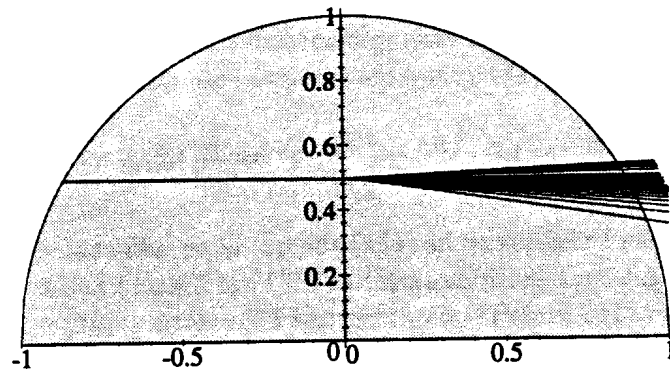
Figure 4: Ray paths for a typical input beam. The center of the beam is at 1/2 the radius of the cane, and the perturbation has the sinusoidal form of (1).
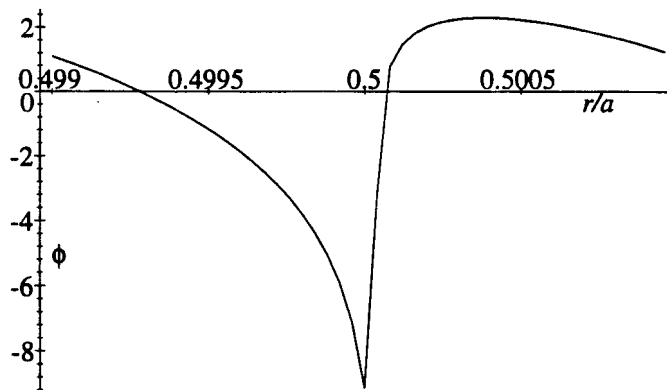
Figure 5: Exit angles for a typical input beam. The center of the beam is at 1/2 the radius of the cane, and the perturbation has the sinusoidal form of (1).

physical width of the beam and the ray paths were computed. One of the programs (written in C) used to compute the paths is given in appendix B. A representative plot is shown in Figure 4.

We can also determine the exit angles as a function of offset using this approach. For the rays in Figure 4, we found the plot of $\phi(t)$ given in Figure 5. Interestingly, we found that the form of $\phi(t)$ varied little across the cane. The layer structure itself dominated the function.

To see how the form of the perturbation affected the data, we also plotted exit angles as a function of t for various forms of the perturbation. The results are shown in Figure 6. The plot labeled sine was a simple sine function as in (1). The plot labeled sawtooth was created from a sawtooth curve with unit amplitude and the same wavelength as the sine in (1). The curve labeled physical was a piecewise linear approximation to the data shown in Figure 2, and the plot labeled Fourier was a four term Fourier approximation to the the piecewise linear function. Although the form of the perturbation can affect the output data, we see that the overall structure
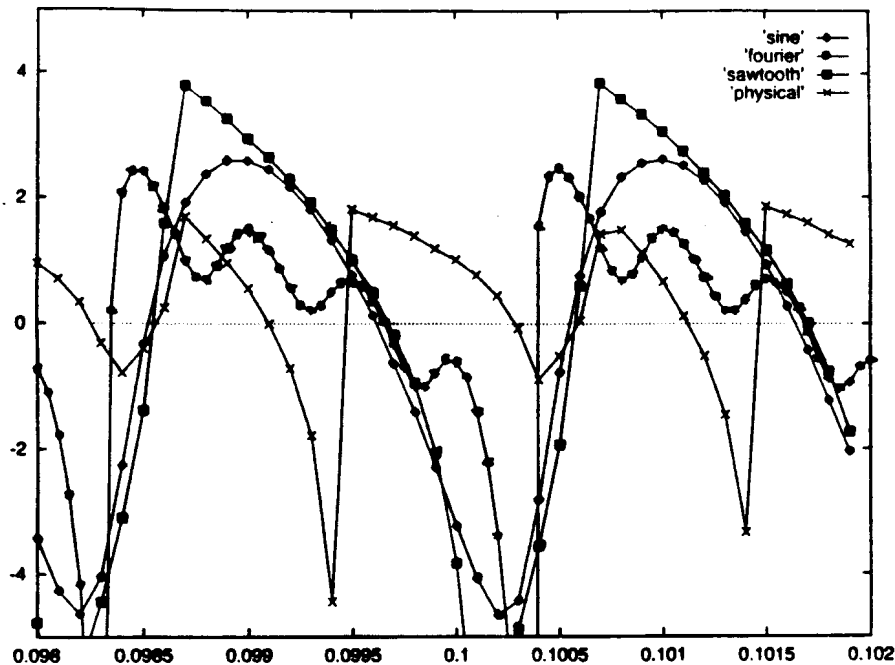
9

Figure 6: Plots of $\phi(t)$ for different forms of perturbation. All had the same amplitude and wavelength, but differed in functional form.

of the perturbation is most relevant, i.e. how many local extrema are present in an oscillation and the wavelength of the oscillation. The smoothness of the perturbation also played a minor role. We saw that smooth functions could cause arbitrarily large exit angles, but these occurred for a very small number of initial conditions (ray paths), and so would be less likely to be observed in a measurement.

Another series of experiments was performed using the paraxial approximation given in (8). These simulations showed good agreement to those using the full equations. One result of these simulations was an "intensity" plot which was obtained by finding the concentrations of ray paths. This is shown in Figure 7. To generate this plot 100 values of the deflection were calculated in an interval of one wavelength of the perturbation (0.02 in this case). The tan(ϕ) axis was partitioned and the number of samples falling in each bin was counted. This was repeated for t values increasing from $t = .01a$ to a in increments of $a/50$. The intensity is greatest where the slope of tan(ϕ) is smallest. Although the layer structure causes a complicated pattern for each layer, it may be possible to invert the data based on

10
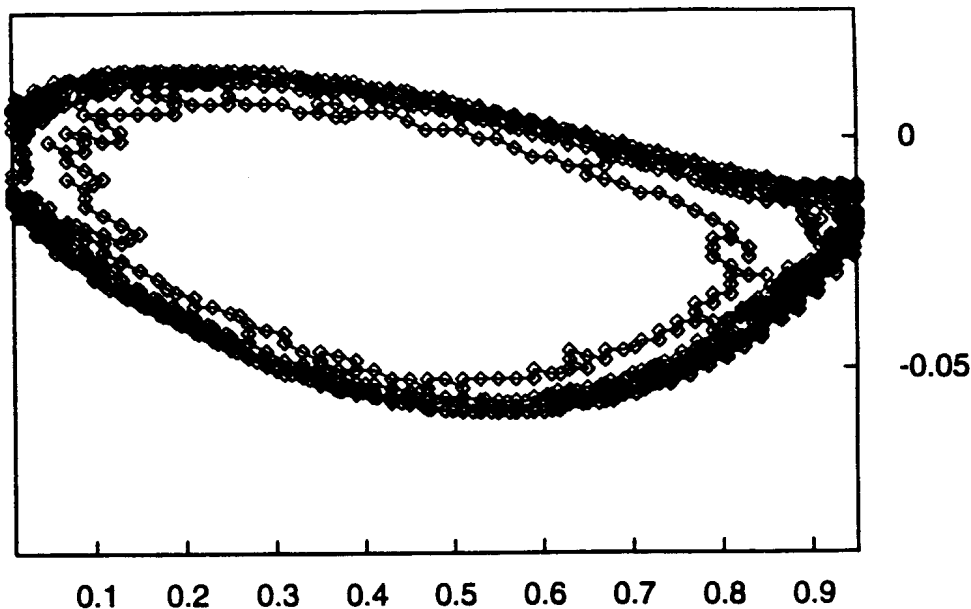
Figure 7: An "intensity" plot found by looking at the densities of the exit angles.

the envelope, but this has not been investigated.

From these and other similar experiments, we were able to conclude the following:

- There is a pronounced focusing effect in each layer near the vertical centerline, since this where the rays are parallel to the contour lines of $n(r)$ and sensitive glancing incidence occurs. In fact, it can be shown using the ray equations, (6) and (7), that a caustic is formed inside each oscillatory band.

- The oscillatory structure is unimportant away from the vertical centerline of the cane. This is supported by the asymptotic analysis of the next section.

- The paraxial approximations and the resulting Abel equation seem to give reasonable agreement to the full ray equations of (6) and (7).

- The layer structure plays a dominant role in the final data. The patterns produced by a layer are fairly independent of the offset of the

incoming beam. However, it may be possible to determine the desired profile from some envelope of the data.

- The basic form of the layer structure is important, but the finer details may not be.

4   Asymptotic Analyses

4.1   Matched Asymptotic Expansions

We again consider (6) and (7) for an incoming horizontal ray at $r = a$ with vertical offset t, which corresponds to $\theta = \pi - \sin^{-1}(t/a)$. This gives $c = -t n_2$ since $n(a) = n_2$. Dividing the equations gives

$$\frac{d\theta}{dr} = \pm \frac{t}{r \left(\frac{r^2 n^2(r)}{n_2^2} - t^2 \right)^{1/2}} \, , \tag{15}$$

where we choose the negative sign for an incoming ray and the positive sign for an outgoing ray. A ray changes from incoming to outgoing at $r_{\min}(t)$ which occurs when $dr/ds = 0$ so from (6) $r_{\min}(t)$ is the largest root of

$$rn(r) = tn_2 \, . \tag{16}$$

We integrate (15) from $r = a$, $\theta = \pi - \sin^{-1}(t/a)$ to $\theta_{\min}(t)$ (which is not a minimum of θ) at $r_{\min}(t)$ using the minus sign to find

$$\theta_{\min} = \pi - \sin^{-1}(t/a) - \int_{r_{\min}(t)}^{a} \frac{t \, dr}{r \left(\frac{r^2 n^2(r)}{n_2^2} - t^2 \right)^{1/2}} \, . \tag{17}$$

By symmetry, the ray will exit at $r = a$ with $\theta = \sin^{-1}(t/a) + 2(\theta_{\min} - \pi/2)$. The deflection angle $\phi(t)$ is the amount that the exiting value of θ is below the input value in the positive direction $\sin^{-1}(t/a)$, so

$$\begin{aligned}
\phi(t) &= 2 \left(\frac{\pi}{2} - \theta_{\min} \right) \\
&= 2 \left[\int_{r_{\min}(t)}^{a} \frac{t \, dr}{r \left(\frac{r^2 n^2(r)}{n_2^2} - t^2 \right)^{1/2}} - \cos^{-1}(t/a) \right]
\end{aligned} \tag{18}$$

We can model a cane with no oscillations with $n(r) = n_2(1 + \Delta\hat{n}(r))$ where $\Delta \ll 1$. If we substitute this into (18) and take care with some near singular behavior in the integral, we find that $r_{\min}(t) = t + \mathcal{O}(\Delta)$ and ϕ is given by (11), and the Abel approximation of (13) is valid.

For the full problem, we write

$$n(r) = n_2 \left[1 + \Delta\hat{n}(r) + \epsilon\Delta\tilde{n}(r) \right] \, .$$

Now the problem is divided into two regions, an outer region, away from $r = r_{\min}(t)$ where the rapid fluctuations cancel and an inner region near $r = r_{\min}(t)$. In the outer region, the leading order contirbution is identical to that found above

$$\phi_{\text{outer}} = -2 \int_t^a \frac{\Delta \hat{n}'(r)}{\sqrt{r^2 - t^2}} \, dr \, . \tag{19}$$

The inner region is more complicated. First we introduce the quantity $\hat{r}_{\min}$ as the solution of

$$[1 + \Delta \hat{n}(\hat{r}_{\min})] \, \hat{r}_{\min} = t \, ,$$

i.e. the minimum radius for the problem without oscillations. Since $\Delta \ll 1$ this can easily be solved as

$$\hat{r}_{\min} = t - t \Delta \hat{n}(t) + \mathcal{O}(\Delta^2) \, . \tag{20}$$

The true value of $r_{\min}$ is found by solving

$$[1 + \Delta \hat{n}(r_{\min}) + \epsilon \Delta \tilde{n}(r_{\min})] \, r_{\min} = t \, .$$

There is an interesting response when $r_{\min}$ is a layer or more larger than $\hat{r}_{\min}$. This occurs when the spatial scale of the fluctuations is the same size as its magnitude, $\epsilon \Delta$. Thus, the rescaling for the inner problem is given by

$$r = \hat{r}_{\min} + \epsilon \Delta \rho \tag{21}$$

The closest approach to the origin by the ray will be given by $\rho = \rho_{\min}$ where $\rho_{\min}$ satisfies

$$\rho_{\min} + t \tilde{n}(t - \Delta \hat{n}(t) + \epsilon \Delta \rho_{\min}) = 0 \, ,$$

where an $\mathcal{O}(\Delta)$ term has been ignored since $\Delta \ll 1$. Now we can compute the deflection in the inner region as

$$\phi_{\text{inner}} = \sqrt{\frac{2\epsilon\Delta}{t}} \lim_{\rho \to \infty} \left[\int_{\rho_{\min}}^r ho\frac{d\rho}{\sqrt{\rho + t\tilde{n}(t - \Delta\hat{n}(t) + \epsilon\Delta\rho)}} - \frac{1}{2}\sqrt{\rho} \right] \, . \tag{22}$$

From this analysis, we can make the following conclusions:

- The deflection away from the vertical centerline of the blank is $\mathcal{O}(\Delta) = \mathcal{O}(\frac{n_2 - n_1}{n_2})$.

14

- The deflection that occurs near the center of the blank is upwards and has size $\mathcal{O}(\sqrt{\epsilon\Delta})$.

- There are no inner deflections for small t because $r\,n(r)$ is monotonic there.

- There are no inner deflections near the outer edge because $\tilde{n} \to 0$ there.

All of these conclusions are corroborated by the numerical experiments.

4.2 Is geometrical optics valid?

The question arises as to whether it is appropriate to use geometrical optics in this probelm because of the fine structure of the layers. The following analysis gives a criterion to determine the validity of the use of geometrical optics for this problem.

Suppose the index of refraction in a dielectric is given by

$$n = 1 + \epsilon\tilde{n}(r/\epsilon)\,,$$

where $0 < \epsilon \ll 1$ represents the wavelength of the perturbation to the base index. The reduced wave equation (Helmholtz equation) for the light waves

$$\triangle u + k^2 n^2 u = 0$$

becomes

$$\triangle u + k^2(1 + 2\epsilon\tilde{n}(r/\epsilon))u = 0\,. \tag{23}$$

Now, we assume that waves are propagating primarily in the x direction, so $u = \psi(x,y)e^{ikx}$. Upon substitution into (23), we get

$$\psi_{xx} + \psi_{yy} + 2ik\psi_x + 2\epsilon k^2\tilde{n}(r/\epsilon)\psi = \mathcal{O}(\epsilon^2)\,. \tag{24}$$

Now we rescale the independent variables near the vertical centerline of the fiber, $x = 0$, $y \approx t$, the offset of the beam initially, since that is where the most refraction takes place.

$$y = t + \epsilon\tilde{y}\,, \quad x = \epsilon^{1/2}\tilde{x}\,, \quad r = t + \epsilon\left(\tilde{y} + \frac{\tilde{x}^2}{2t}\right) \tag{25}$$

When these are substituted into (24), we find

$$\epsilon\psi_{xx} + \psi_{yy} + \epsilon^{3/2}k2i\psi_x + 2\epsilon + 2\epsilon^3 k^2\tilde{n}\left(y + \frac{x^2}{2t}\right)\psi = \mathcal{O}(\epsilon^4)\,, \tag{26}$$

where we have multiplied by ϵ^2 and dropped the tildes from the new variables. The ψ_{xx} term is always $o(1)$, but a key balance for the other terms occurs when $\epsilon^3 k^2 = 1$, for then the leading order terms of (26) give

$$\psi_{yy} + 2i\psi_x + 2\bar{n}\left(y + \frac{x^2}{2t}\right)\psi = 0 \,. \tag{27}$$

If $\epsilon^3 k^2 \ll 1$ then the layers are too small to be seen by the waves and the only result is their net effect (which is very small). If $\epsilon^3 k^2 \gg 1$ then the wavelength of the input beam is much smaller than the oscillations of the index of refraction and standard geometrical optics is valid. For a typical cane measurement, typical data is

$$
\begin{aligned}
\text{radius} \quad &= \quad a = 10\text{mm} = 10,000\mu\text{m} \\
\text{wavelength} \quad &= \quad \lambda = 633\text{nm} = .633\mu\text{m} \\
\text{perturbation} \quad &= \quad \tilde{n}(r) = A\sin\left(\frac{2\pi r}{L}\right)
\end{aligned}
$$

where L varies between 46 and 71. Thus, we have $\epsilon = 60/20,000\pi \approx 10^{-2}$ and $k = 10,000/.633 \approx 1.5 \times 10^4$ so $\epsilon^3 k^2 \approx 2.5 \times 10^3$ which suggests that geometrical optics may be valid for this problem. If geometrical optics is not valid, then the analysis of the previous section is still valid, but now (27) must be used for the inner problem.

5 Conclusions

The following conclusions and comments were obtained by the MPI '95 study group for this problem.

- Information about the layer structure will be needed before an accurate inversion of the data can be obtained. It is not known at this time how much detail about the structure is necessary.

- Most of the refraction occurs near the vertical centerline of the core being probed. This is where the incoming rays are nearly tangent to the lines of constant $n(r)$.

- The problem is in some sense ill-conditioned since the noise swamps the desired data. However, if the noise can be removed, it may still be possible to recover the background profile. It may be possible to exploit the work on waves through random media, but this will take more work.

- Reflections inside the cane have been ignored. The data in Figure 2 suggests that sharp interfaces may be present in the canes that will cause reflections. According to some calculations, the key angle is approximately $3°$, which also figures prominently in experimental data.

- An alternate measuring technique examining the reflections from the end of the cane was also suggested, but its implementation looked to be too expensive.

- (added during the report write up) It may be possible to exploit some global characteristics of the data to determine the background profile. Unfortunately, time did not exist to explore this possibility during MPI '95, but it should be examined.

6 Working Group

The following participants contributed to this problem: John Abbott, Jay Bourland, Jon Chapman, Ellis Cumberbatch, Bill Dold, Steven Epstein, Alistair Fitt, Donald French, John Hinch, John King, Colin Please, Jorge Sobehart, Warren Weckesser, Tom Witelski, Vadim Zharnitsky. If you have questions or comments about this report, please contact Jay Bourland, jayb@MATH.ColoState.EDU.

A Notation

r   Position vector for a point in space.

r, θ Polar Coordinate variables. r is measured from the centerline of the cane and $\theta = 0$ is parallel to the incoming light ray pointing at the exit side. $[n(r)]$ Index of refraction of the cane.

n_1 Index of refraction at the center of the cane. $[n_2]$ Index of refraction at the outer edge of the cane. Generally, $n_1 > n_2$.

$n_p(r)$ The unperturbed (desired) index profile.

ϕ Deflection angle of the light ray measured with the same orientation as the polar angle variable θ.

α Angle between and incoming ray and a tangent line to circle centered at $r = 0$.

s Arclength parameter of a light ray.

c Constant of integration for the ray paths determined by the initial slope of the ray.

a Radius of the cane.

t Offset of incoming light ray from the centerline of the cane.

ϵ Amplitude (relative to $n_p(r) - n_2$) of the perturbations to the index of refraction for the cane.

N Number of oscillatory layers within the cane.

L Distance from the observation screen to the center of the cane.

$y_{\mathrm{obs}}(t)$ Offset of the light ray at the observation screen.

B Program Listing

```
#include<stdio.h>
#include<math.h>

#define sqr(x) ((x)*(x))
#define fabs(x) ((x)>0.0 ? (x) : -(x))
#define max(a,b) ((a)>(b)? (a):(b))
#define sgn(x) ((x)>=0.0 ? 1.0 : -1.0)
#define pi M_PI

double s,R[2];   /* full axi-symmetric cylindrical */          10
double work[6];
double s1,Y[2]; /* paraxial approx */
double n();
double np();
double t,a,c;
double n2,n1;
double eps,N;
double sign= -1.0;    /* !!!!!!!!!!!!!!!! */
double sign1=-1.0;
double R1[1];                                                  20
double s2;
void getparams(double *, double *,double *);
double variation(double);

double h;

int F();

/*——— parameters ———*/
FILE *out;                                                     30
FILE *out2;

main()
{
        int i;

        double uu;
```

```
        double  rp,xx,yy;
        double  xx1,yy1;                                           40
        double  ang1,npaths,beamwidth,beamcenter;

getparams(&npaths,  &beamwidth,  &beamcenter);
/* actually the universal parameters are set as well */

t= beamcenter  −  beamwidth/2.0;
out=fopen("paths","w");
out2 = fopen("angles","w");
while(t<  beamcenter+beamwidth/2)
{                                                                 50
        sign= −1.0;
        xx= −sqrt(sqr(a)−sqr(t));
        yy=t;
        rp= −a*xx/yy;
        c= −t*n2
/*——— initial conditions ———*/
        R[0]=a;   /* r */
        R[1]=atan2(yy,xx); /* phi */
        s=0.0;
        fprintf(out,"%f  %f\n",  R[0]*cos(R[1]),R[0]*sin(R[1]));   60
        h=1e−4;

        do
        {
                rk(R,s,h,2,F,work);
                s+=h;
                i++;
                if(!(i%100))
                {
                        i=0;                                      70
                        fprintf(out,"%f  %f\n",
                        R[0]*cos(R[1]),R[0]*sin(R[1]));
                }
        }while(R[0]<1.1*a);
        printf(" *** %f \n",t);

        fprintf(out,"\n");
```

```
xx=R[0]*cos(R[1]);
yy=R[0]*sin(R[1]);                                                          80
rk(R,s,h,2,F,work);
xx1=R[0]*cos(R[1]);
yy1=R[0]*sin(R[1]);
fprintf(out2,"%g  %.16g \n",t,atan2(yy1-yy,xx1-xx)*180.0/pi);

fflush(out);
fflush(out2);

t+=beamwidth/npaths;
}                                                                          90
fclose(out);
fclose(out2);
}


rk(x,tt,h,n,F,work)
/* fourth order general Runge-Kutta for a system of ODEs */
double *x;
double *work;  /* array of 3*n doubles */
double tt,h;
int (*F)();                                                               100
int n;
{
        int i;
        double t;
        double h2=h/2.0;
        double h6=h/6.0;

        double *k1,*k0;
        double *x1;
        k0=work;                                                         110
        k1=k0+n;
        x1=k0+2*n;

        t=tt;
        F(x,k1,t);

        for(i=0;i<n;++i)
        {
```

```
                    x1[i]=x[i]+h2*k1[i];
                    k0[i]=k1[i];                           120
        }
        t=tt+h2;
        F(x1,k1,t);

        for(i=0;i<n;++i)
        {
                    x1[i]=x[i]+h2*k1[i];
                    k0[i]+=2.0*k1[i];
        }
        t=tt+h2;                                           130
        F(x1,k1,t);

        for(i=0;i<n;++i)
        {
                    x1[i]=x[i]+h*k1[i];
                    k0[i]+=2.0*k1[i];
        }
        t=tt+h;
        F(x1,k1,t);
                                                           140
        for(i=0;i<n;++i)
                    x[i]+=h6*(k0[i]+k1[i]);
    /* don't update time */
}


F(X,KK,t)
double *X,*KK,t;
{
        double r,phi;
        double rp,phip;                                    150
        double root;

        r=X[0];
        phi=X[1];
        root=sqr(n(r))-sqr(c/r);
        if(root<0.0) sign*= -1.0;

        /* a ray with rp<0 */
```

```
        rp=  sign*sqrt(fabs(root))/n(r);
        phip=c/(n(r)*sqr(r));                                              160

        KK[0]=rp;
        KK[1]=phip;
}

double n(r)
double r;
{
        if(r>a) return(n2);
        return(n2+(n1-n2)*(1.0-sqr(r/a))*(1.0+eps*variation(r)));  170
}

double np(r)
double r;
{
        return(-2.0*r/sqr(a)*(n1-n2));
}

void getparams( double *np, double *bw, double *bc)
{                                                                          180
  a  = 1.0;
  N  = 500;
  n1 = 1.47;
  n2 = 1.45;
  eps = 0.0;

  printf("Enter width of beam (as a fraction of radius) >>   ");
  scanf("%lf", bw);
  printf("\nEnter center of beam (as a fraction of radius) >> ");
  scanf("%lf", bc);                                                        190
  printf("\nEnter the number of ray paths to compute >> ");
  scanf("%lf", np);
}

double variation ( double r)
{
/* sin plus extra
return((2.0/pi)*sin(2.0*pi*N*r/a) - (1.0/pi)*sin(4.0*pi*N*r/a)
```

23

```
                 + (2.0/(3.0*pi))*sin(6.0*pi*N*r/a)
                 - (1.0/(2.0*pi))*sin(8.0*pi*N*r/a));            200
/* */

/* double hump sawtooth */

double A,B,C,yB,yC, x;

A  = .1;
B  = .5;
C  = .7;
yB = .5;                                                        210
yC = .3;


x = r*N  -  floor(r*N);

if (x < A)
      return(2.0*((1.0 - x/a) - .5));
else if ( x < B)
      return(2.0*(((x - A)/(B-A) * yB) - .5));
      else if (x < C)
            return(2.0*(( yB - (x-B)/(C-B)*(yB-yC)) - .5)); 220
      else
            return(2.0*(( yC + (x-C)/(1.0-C)*(1-yC)) - .5));
/* */

/* simple sine wave
return(sin(2.0*pi*N*r/a));
*/

/* single sawtooth
                                                               230
return(asin(sin(2.0*pi*N*r/a)));
/**/
}
```

References

[1] Marcuse, Dietrich, *Principles of Optical Fiber Measurement*, Academic Press, 1981, New York.

[2] Keller, Joseph B., *Asymptotic Methods for Partial Differential Equations: The Reduced Wave Equation and Maxwell's Equations*, preprint.